ORIGINAL ARTICLE

CrossMark

Experimental investigation on the stress sensitivity of permeability in naturally fractured shale

Diansen Yang[1,2] · Wei Wang[1,2] · Kang Li[1,2] · Weizhong Chen[1,3] · Jianping Yang[1] · Shugang Wang[3]

Abstract

In this paper, we present an experimental investigation regarding the stress sensitivity of permeability in naturally fractured shale. Gas permeability tests were performed on the fractured cylindrical shale samples under loading and unloading conditions. Different hydrostatic stress and gas pressure levels were chosen to investigate the dependence of permeability on stress. The permeability of the fractured shale decreases with increasing hydrostatic stress, re-increases during unloading and is irreversible during loading and unloading processes. The gas pressure exhibits a significant effect on the permeability in comparison with the hydrostatic stress. Small gas pressure changes (e.g., 2 MPa) induce a comparable change in permeability with a large hydrostatic stress change (e.g., 40 MPa). The gas pressure gradient on the permeability will be discussed. The fracture aperture was estimated by recording the volume change during loading and shows that the aperture change is consistent with the permeability evolution during loading, which is more complicated at a higher hydrostatic stress value. The roughness of the fractured surface was also analyzed and will be discussed in combination with the permeability evolution.

Introduction

In recent years, shale gas has been considered to be a clean energy in many countries, which can be utilized to help solve the energy crisis and reduce the greenhouse effect. However, only a few countries (e.g., United States, Mexico, and China) have realized the commercial exploitation of shale gas because of a series of difficulties, among which the low permeability of shale is an important factor that restricts gas production. To enhance the production of shale gas, two key technologies (i.e., horizontal drilling and hydraulic fracturing) have been significantly advanced. Horizontal drilling can create a maximum borehole surface area, and hydraulic fracturing can provide a high conductivity pathway by increasing the artificial fractures around the well bores. The permeability of natural or induced fractured shale is crucial to understanding the production performance after hydraulic fracturing operations, and hence, it is an important parameter to evaluate the production of shale gas. Therefore, permeability characterization is an important issue in the shale gas productivity evaluation.

A significant number of studies (Carey et al. 2015; Chen et al. 2015; Cho et al. 2013; Gale et al. 2007; Gutierrez et al. 2010, 2015; Yang et al. 2017; Zhou et al. 2016; Zhang et al. 2013) have been conducted to investigate the permeability of intact shales and fractured shales. The results show that the permeability of both intact shale and fractured shales strongly depends on the applied stresses. The stress dependence of the permeability of intact rock is often described by an exponential relationship or a power law between the permeability and porosity (Dong et al. 2010; Wang et al. 2011; Yang et al. 2017). The influence of stresses on the permeability of fractured shale is more significant than that of intact shale (Gutierrez et al. 2015). The permeability of fractured shales depends on both the applied stress and fracture surface. To investigate the fracture permeability, fractures are often artificially created through tensile testing (e.g., Brazilian test) or the saw cut. Permeability tests are usually conducted in a triaxial cell with or

✉ Jianping Yang
  jpyang04@163.com

1 State Key Laboratory of Geomechanics and Geotechnical Engineering, Institute of Rock and Soil Mechanics, Chinese Academy of Sciences, Wuhan 430071, Hubei, China

2 University of Chinese Academy of Sciences, Beijing 100049, China

3 Geotechnical and Structural Engineering Research Center, Shandong University, Jinan 250061, Shandong, China

without a shear displacement (Hofmann et al. 2016) or shear box (Vogler et al. 2016; Xiong et al. 2011). It is found that the fracture permeability will decline with increasing confining stress, which compacts the fracture aperture, while the fracture permeability will increase under a high shear stress, which can increase the fracture width due to an offset in the two fracture surfaces. Several researchers have found that cyclic loading and unloading significantly affects permeability and induces a notable hysteresis effect (Gutierrez et al. 2015; Smart et al. 2001; Lu et al. 2018a, b). Although the effective stress principle is widely applied to consider the effect of pore pressure on permeability, the effective stress coefficient is often difficult to determine. Moreover, the hydromechanical coupling phenomenon cannot be ignored in many cases (Figueiredo et al. 2015; Lu et al. 2018a, b). Thus, it is necessary to further investigate the effect of pore pressure on the permeability of fractured shales. Because it is challenging to obtain natural fractures in standard samples, there are relatively few studies addressing on the permeability of natural fractured shale (Vogler et al. 2016; Ye et al. 2017). This paper will present an experimental study on the permeability of naturally fractured samples under coupled hydromechanical loading and unloading conditions.

Material and sample preparation

In this study, the tested material is Longmaxi (LM) shale collected from the outcrop shale block of the Lower Silurian Longmaxi (LM) shale formation located in Qianjiang, southeast of Chongqing, China. The Longmaxi shale formation comprised of dark gray to black graptolite shale, carbonaceous shale, siliceous shale, silty shale, and argillaceous siltstone (Yang et al. 2017). The organic content of shale is larger than 0.5% with a mean TOC of 2.54%. The LM shales are mainly composed of clay (54%), quartz (33%) with minor quantities of pyrite and feldspar. The grain density of the shale sample was approximately 2.72 g/cm^3 with a total porosity of 0.25–3.25%, and the initial water content was less than 4%. The shale block was naturally fractured, and three cylindrical samples with diameters of 25.0 mm and lengths of 50.0 mm were drilled from this block. The coring orientation was chosen to allow the natural fractures to align parallel to the longitudinal axis of the cylindrical samples (see Fig. 1).

Methods and procedures

Experimental method

To measure the permeability of the fractured shale samples, a steady-state method was preferred because it has a better accuracy for measurements of high permeability values. To avoid the interaction between water and shale (Zhang et al.
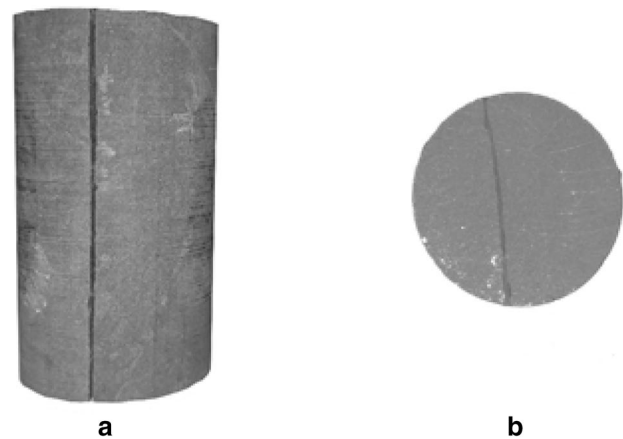

Fig. 1 Photos of natural fractured shale

2013), the dry nitrogen gas was used as the fluid for the gas measurements. The gas permeability under a constant pressure gradient resulting in a constant flow rate was estimated using the following formula (Davy et al. 2007):

$$K = \frac{\mu L}{A} \frac{2P_0 q}{P_2^2 - P_1^2},$$ (1)

where P is the pressure across the sample (Pa), subscripts 0, 1 and 2 denote the average, upstream and downstream pressures, respectively, μ is the viscosity of the gas (Pa.s), q is the flow rate (m^3/s), L is the length of the sample (m), and A is the cross-sectional area of the sample (m^2). This solution is based on Darcy's law and assumes that the ideal gas law is valid.

To explain the fracture permeability test, the fracture hydraulic opening "e" is often used and is expressed as follows for an ideal gas (Su et al. 2017):

$$e = \sqrt[3]{\frac{24\mu P_0 q L}{D(P_2^2 - P_1^2)}},$$ (2)

where D (m) is the diameter of the sample. The hydraulic opening "e" can be derived from the permeability K and both can express the transmissivity of the fracture. In this study, the permeability K is used.

The fractured shale sample was placed in a triaxial cell that was designed for cylindrical samples with diameter of 25 mm. The axial and confining stresses up to 56 MPa were independently applied using two ISCO-260D pumps with control up to ± 1 kPa. The gas pressure in the upstream is controlled by an ISCO-500D pump. The flow rate was measured using an improved bubble gas flow meter. The gas volume was equal to the volume of water extruded from bottle A to bottle B, in which the increased weight was recorded

continuously (see Fig. 2). The flowmeter was connected to the outlet of the fluid pipelines and the atmosphere. The apparatus was placed in an oven, where the temperature was controlled, and its variation was within ± 0.1 °C during testing.

Experimental procedure

To eliminate water–rock interactions, the fractured shale samples were first dried in the oven for 24 h and then placed in the triaxial cell. The air in the sample fracture and connecting pipes was removed through a vacuuming procedure before permeability test. All tests were conducted at a constant temperature of 25 °C. To evaluate the stress-dependent permeability of the fractured shale, different hydrostatic stresses and gas pressures were applied on the fractured sample. Generally, four gas pressures (i.e., 0.5 MPa, 1 MPa, 2 MPa and 3 MPa) were chosen as the input pressure for the steady-state flow gas permeability measurements. The outlet pressure is kept as atmospheric pressure. The pressures were constant during the mechanical loading and unloading processes. Considering the in situ stress of Lower Silurian Longmaxi (LM) shale formation (Ren et al. 2015), the hydrostatic stress in tests progressively increased from 5 to 10 MPa, 20 to 30 MPa, 40 to 45 MPa, and then decreased to 40 MPa, 30 MPa, 20 MPa, 10 MPa and 5 MPa. At each mechanical loading step, the gas permeability was measured. These conditions were adjusted for the three samples, e.g., only three gas pressures were imposed on sample no. 2. The

permeability was then calculated using Eq. (1). The detailed loading paths of these three samples are presented with the experimental results in Fig. 3.

To further investigate the effect of the gas pressure gradient on the permeability, an additional permeability test was performed on sample no. 2. When the gas permeability tests under cyclic loading and unloading finished, the hydrostatic stress and gas pressure were decreased to 20 MPa and 1 MPa, respectively. Then, the gas pressure was successively increased from 1 to 5 MPa under constant hydrostatic stresses (20 MPa, 30 MPa, 40 MPa), and the gas permeability tests were carried out. The measured permeabilities are shown in "Permeability versus gas pressure at a constant hydrostatic stress" section.

Results

Permeability versus hydrostatic stress at a constant gas pressure

The permeability of sample no. 1 at a hydrostatic stress of 5 MPa and a gas pressure of 0.5 MPa is 4.96×10^{-15} m^2 and is much larger than that of sample no. 2 (8.44×10^{-17} m^2) and sample no. 3 (2.82×10^{-16} m^2) under the same stress conditions. The permeability of fractured shale samples is much larger than that of intact shale matrix, which is between 10^{-20} and 10^{-22} m^2 through previous tests (Yang et al. 2017). Thus, the transmissivity of the shale matrix
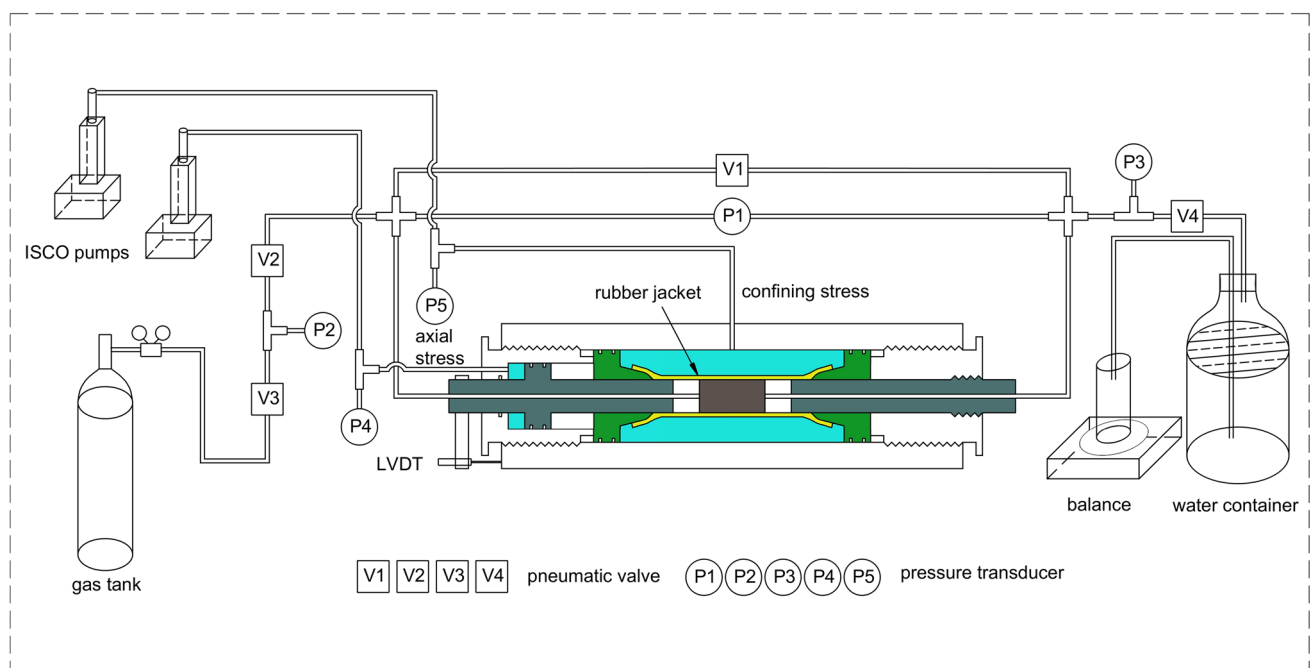
Fig. 2 Schematic of the experimental setup
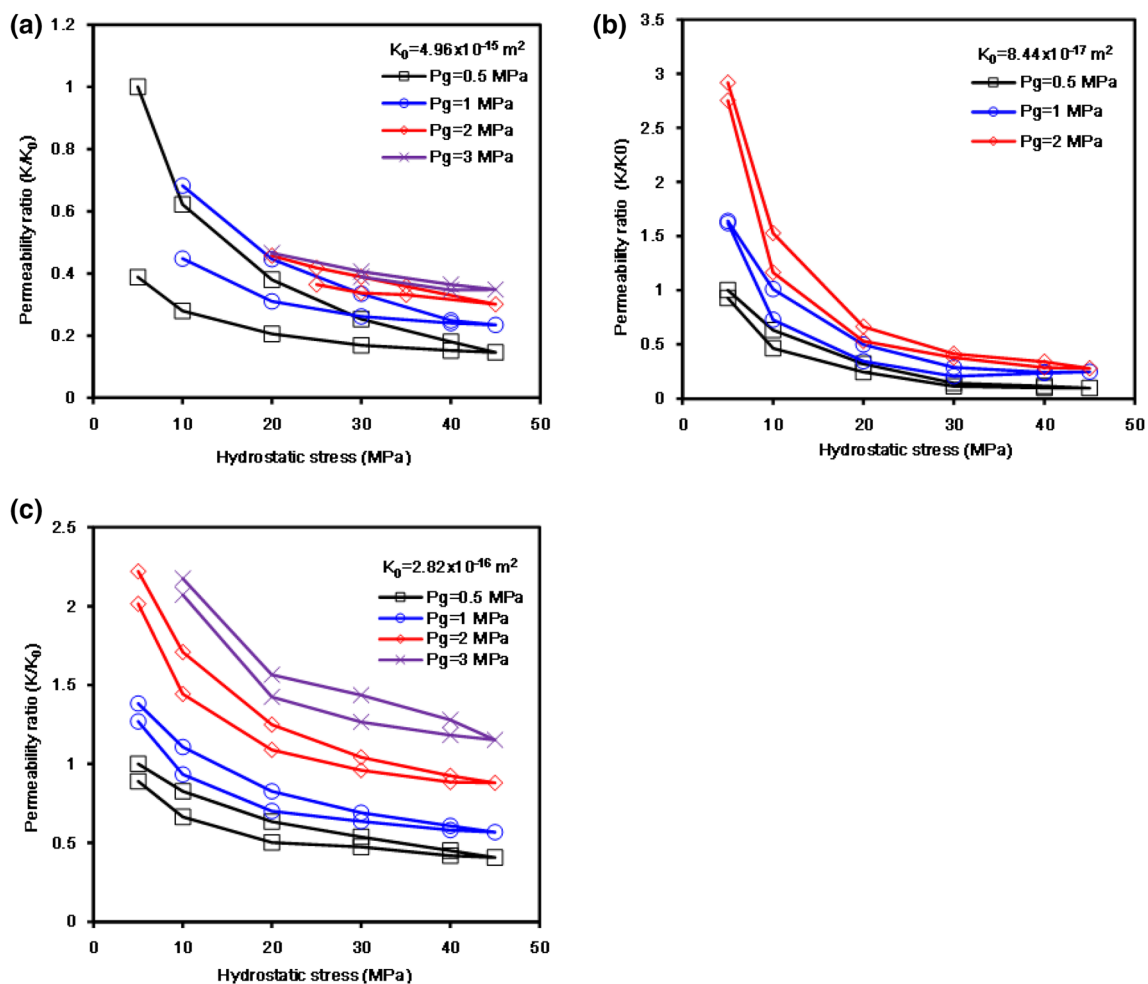
Fig. 3 Permeability ratio versus hydrostatic stress: **a** sample no. 1; **b** sample no. 2; and **c** sample no. 3

is ignored in the following analysis and the gas flow is all attributed to the transmissivity of shale fracture. To clearly describe the evolution in permeability during loading and unloading, the permeability ratio is defined as the ratio between the measured permeability (K) and the initial permeability (K_0) at the initial state (hydrostatic stress = 5 MPa and gas pressure = 0.5 MPa). The evolutions in the permeability ratio for the three samples under different constant gas pressures are plotted in Fig. 3a–c. The results show that the permeability ratio varies similarly for the three samples under constant gas pressures, decreases during loading and re-increases during unloading. Moreover, the ratio is irreversible during loading and unloading. The permeability ratio is also nonlinear during loading, which indicates that the permeability changes decrease with increasing hydrostatic stress. Figure 3a–c shows that the permeability ratios of the three samples are different. Specifically, the permeability ratio varies between 1 and 0.15 for sample no. 1 during loading under a gas pressure of 0.5 MPa, and the ratio varies between 2.92 and 0.28, and between 2.22 and 0.88 during

loading under a gas pressure of 2 MPa for samples no. 2 and no. 3, respectively. Therefore, the dependence of the permeability upon hydrostatic stress is significant and varies for different fractured shales. The difference should be related to the roughness of the fractures and will be discussed in the following with a scanning analysis of the fracture surfaces. Note that the loading and unloading paths were adjusted slightly during the testing of samples no. 1 and no. 3 at a high constant gas pressure (3 MPa) because the permeability of the samples at a low hydrostatic stress (5 MPa) is very high in comparison with that during other stages. Sample no. 2 was not tested at a gas pressure of 3 MPa.

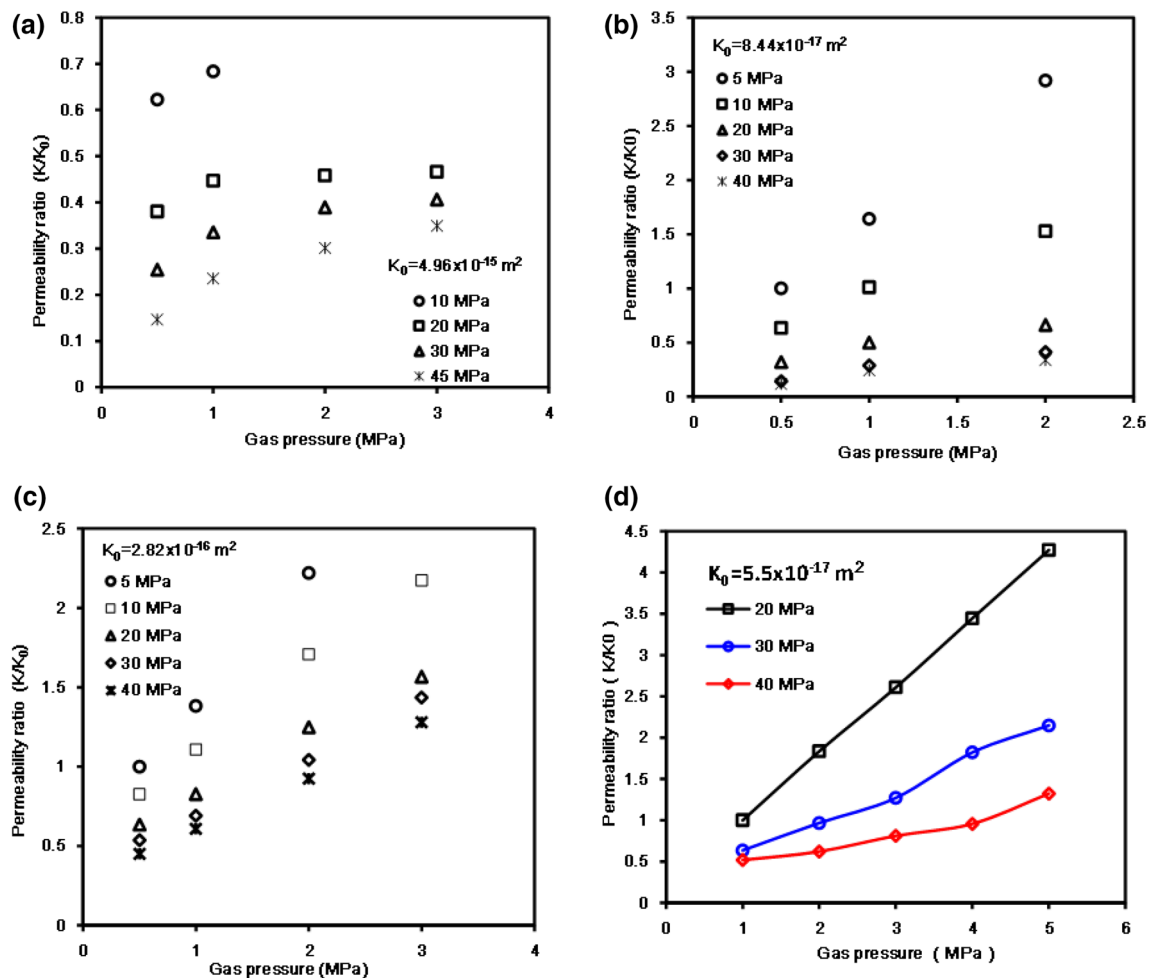## Permeability versus gas pressure at a constant hydrostatic stress

Figure 4 shows the results of the effect of the gas pressure on permeability: the small change in gas pressure induces a notable change in the permeability. To describe this notable effect, the relationship between the gas pressure and

permeability ratio of the samples no. 1, no. 2, no. 3 at different hydrostatic stresses is illustrated in Fig. 4a–d, respectively. It is found that the permeability ratio increases with increasing gas pressure and the evolution of the ratio is also different for the three samples. The relationship between the permeability ratio and gas pressure is quasi-linear for sample no. 3 under different hydrostatic stresses, and it is quasi-linear for sample no. 1 at low hydrostatic stress (5 MPa) and nonlinear under high hydrostatic stress (30 MPa, 40 MPa). For sample no. 2, the relationship between the permeability ratio and gas pressure is quasi-linear and is similar under two different loading paths (i.e., cyclic loading and unloading in Fig. 4b and under a constant hydrostatic stress with increasing gas pressure in Fig. 4d). Such a relationship cannot be simply explained using the effective stress principle, which indicates a similar evolution due to a hydrostatic stress change, as shown in Fig. 5. The effect of gas pressure seems much notable in comparison with that of the hydrostatic stress. For example, the permeability ratio of sample

no. 2 varies from 0.6 to 1.5 when gas pressure increases from 0.5 MPa to 2 MPa at a hydrostatic stress of 10 MPa and also from 1.6 to 0.3 when the hydrostatic stress increases from 5 to 45 MPa for the gas pressure of 1 MPa. This result indicates that the gas pressure induces a larger permeability change compared with the same magnitude of stress change. The increase in gas pressure not only reduces the effective stress but also changes the matching of the two fractured surfaces, which is another important factor influencing the permeability. Moreover, as the gas pressure in the downstream of the test is constant, the high pressure means a high-pressure gradient, which plays an important role in the gas permeability measurement.

Volume change versus hydrostatic stress

The permeability of rock not only depends on the applied stress but is also closely related to the fracture characteristics, such as the aperture, frequency, length, specific

Fig. 4 Permeability ratio versus gas pressure: **a** sample no. 1; **b** sample no. 2; **c** sample no. 3; and **d** sample no. 2 under constant hydrostatic stress
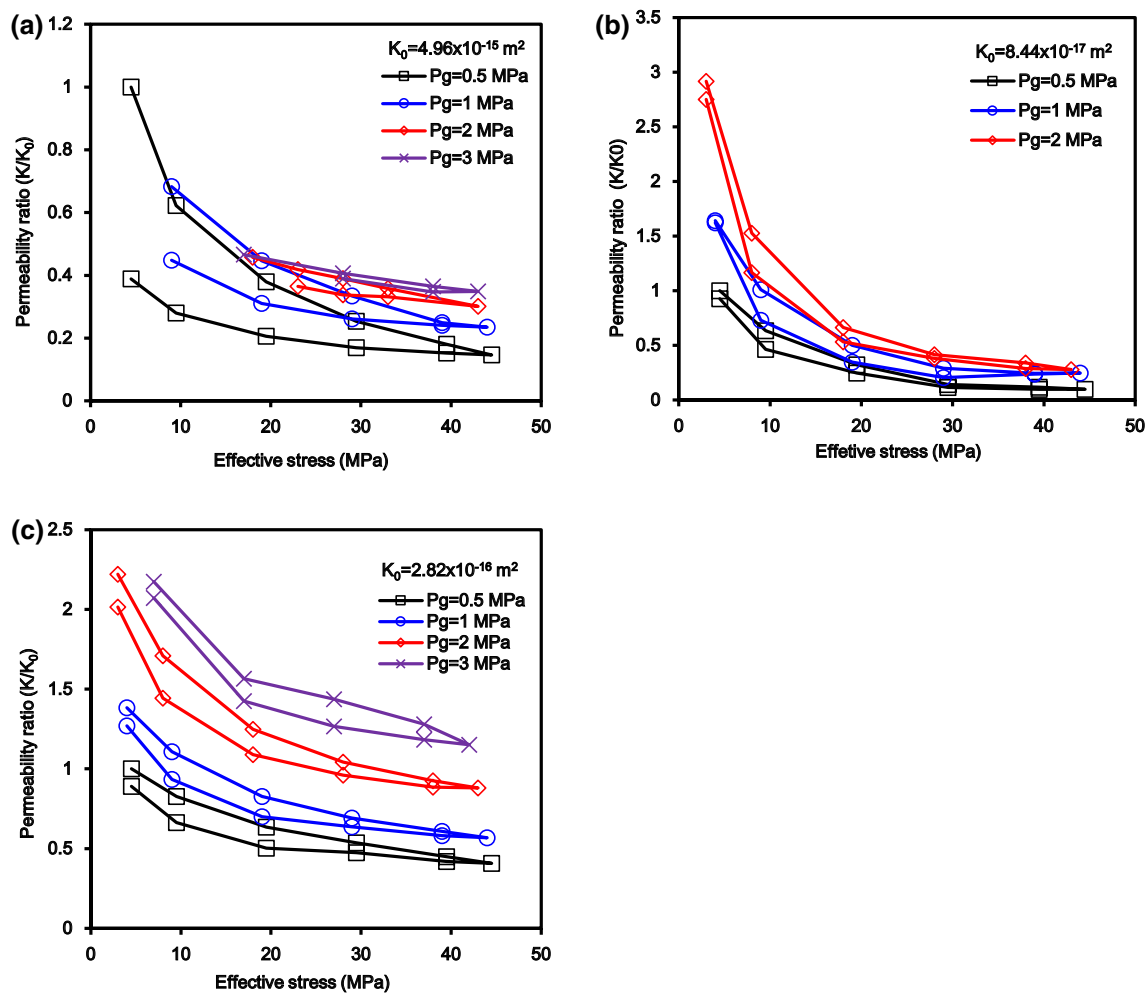
Fig. 5 Permeability ratio versus effective stress (i.e., hydrostatic stress minus gas pressure)

orientation, interconnectivity of the network, filling materials, and features of the fracture surface (Shimi 1995). The volume change is the origin of the permeability variation, and it can be estimated by the measured deformation in the materials. In this study, the fracture aperture change (Δb) of the fractured shale was estimated as the following: $\Delta b = \Delta V/A$, where A denotes the area of the fractured surface and ΔV stands for the volume change in the sample during the loading and unloading processes. Because the fracture surface is close to the center of the sample and is along the axial direction, the area may be estimated by multiplying the diameter and the length of the sample. During testing, the oil volume change around the sample was recorded by the ISCO pump, and ΔV is the difference between the volume change in the fractured shale (ΔV_f) and that of the intact shale with the same size of the tested fractured shale (ΔV_i). The aperture change in sample no. 2 is illustrated in Fig. 6. The aperture change nonlinearly increases with increasing hydrostatic stress, i.e., the aperture change decreases at high

hydrostatic stress. This evolution is consistent with the permeability change during loading (See Fig. 3). It is found that when the hydrostatic stress exceeds 40 MPa for sample no. 2, the aperture change becomes negative, which indicates that the fracture reopen at high stress. This variation could be related to asperity damage and rotation induced by high pressure.

Roughness of the fractured surface

Because rock roughness is a key factor that influences the permeability of fractured rocks (Barton et al. 1985; Hakami et al. 1996; Li et al. 2015), to further investigate the roughness of the fractures, the fracture surfaces of the three samples were scanned using a REVscan 3D scanner with a resolution of 50 µm, since the scanning area is larger than the fracture surface area, the redundant information of the scanning area. The data obtained from REV scan 3D is the space coordinate data, which is recorded as (x, y, z).
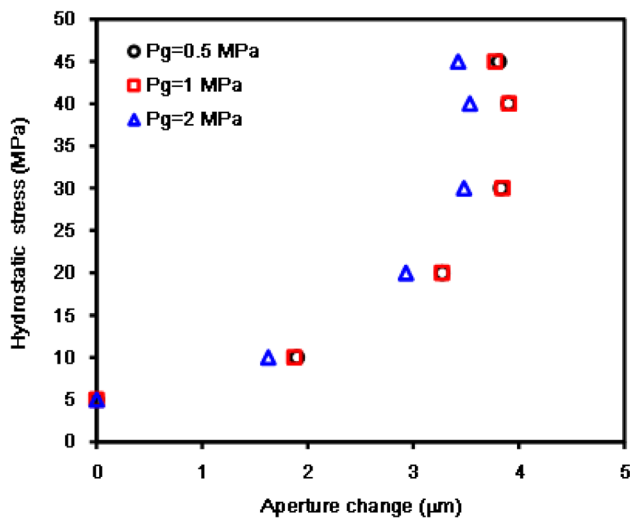
Fig. 6 Aperture change in the fractured shale

The coordinate of "z" represents the height of the surface. To clearly describe the roughness, the height data are compared to a plane that fits the recorded coordinate data best using a least square method. To transform the unstructured coordinate data to a structured 2D grid for 3D surface visualization, the grid data function was employed due to its better precision and adaptability compared with the interp2d function from the interpolate module of the SciPy package. Finally, the Python graph library Plotly was used to visualize the scanned surface. The surface roughness was quantified with the asperity height, which is shown through the heat map. The heat map (Fig. 7) was drawn using the matplotlib library for Python. Figure 7 illustrates that the roughness of the fracture surfaces is very different for the three samples.

The ratio of the total (A_t) to planar (A_p) fracture surface area is considered to be roughness here and is 1.002, 1.001, and 1.01 for samples no. 1, no. 2 and no. 3, respectively. The quantified ratio of roughness shows that a low ratio means a low fracture surface roughness. Sample no. 2 has a smallest ratio, and the initial permeability of the sample is lowest among the three samples. A similar behavior was also found in fractured granite samples (Hofmann et al. 2016). The height variation along the axial direction of the sample at three selected profiles ($Y = 5$, 10 and 15 mm in Fig. 7) is the smallest for sample no. 2 (Fig. 8). Sample no. 3 has the highest ratio, but its permeability is lower than that of sample no. 1. It indicates that the quantified ratio of roughness here is not sufficient for comparison of permeability between different fracture surfaces. The large permeability of the sample no.1 may be related to the initial mismatching when the two parts of the samples were placed in the cell and they were not well matched. Other factors, such as height variation rate, may also influence the transmissivity of fracture surface.

Discussions

The results show that the permeability of natural fractured shale strongly depends on both the hydrostatic stress and gas pressure. Such a dependence has been often found and investigated (Dong et al. 2010; Seidle et al. 1992; Palmer and Monsoori 1998) and is frequently expressed using an exponential law or a power law. The effective stress is often used in these formulae and is defined by $\sigma' = \sigma - bp$, where σ' is the Cauchy stress tensor, p is the pore pressure and b is Biot's coefficient. An increase in hydrostatic stress or a decrease in pore pressure will compress the rock and reduce the effective porosity or fracture aperture and lead to a decrease in the permeability. This point is supported by the obtained results (Figs. 3, 4), but the effective stress principle cannot fully explain the fact that a small gas pressure change induces a high permeability variation in comparison with the large hydrostatic stress change as indicated above. This finding means that the effect of gas pressure on the permeability is larger than that of the hydrostatic stress when changed at the same magnitude and is contrary to the effective stress principle. Because Biot's coefficient is often less than 1, the contribution of the gas pressure on the effective stress should be less than that of the hydrostatic stress. This effect is possibly due to that fact that the gas permeability of the fractured shale can be influenced by not only the stress but also other factors, e.g., gas slippage, surface roughness, and shear deformation. The high gas pressure can reduce the gas slippage effect, which could be dominant at low gas pressures for intact tight rocks. In this study, the gas slippage effect is believed to be eliminated for the significant effect of gas pressure on the gas permeability relative to the hydrostatic stress. Fracture permeability could be varied due to the change of fracture surface roughness. However, the roughness change, which is closely related to the variation of effective stress, also cannot explain the dominant effect of gas pressure on the permeability. Mismatch between the rough fracture surfaces could greatly influence the fracture permeability (Wu et al. 2017; Ye et al. 2017). It is not a plausible explanation that small gas pressure change would induce the same mismatch compared to a much larger confining pressure under hydrostatic stress state. In Su et al. (2017) found a notable impact of the pressure gradient on the fracture hydraulic opening. Su and coworkers determined that the change in the gas permeability of the fracture as function of pressure gradient can be explained by the change in the flow regime inside the fracture. The turbulence of the flow increased the interaction of the gas flow with the fracture walls. In this study, the flow rate is recorded and it is found that the relationship between the flow rate and gas pressure gradient during testing is
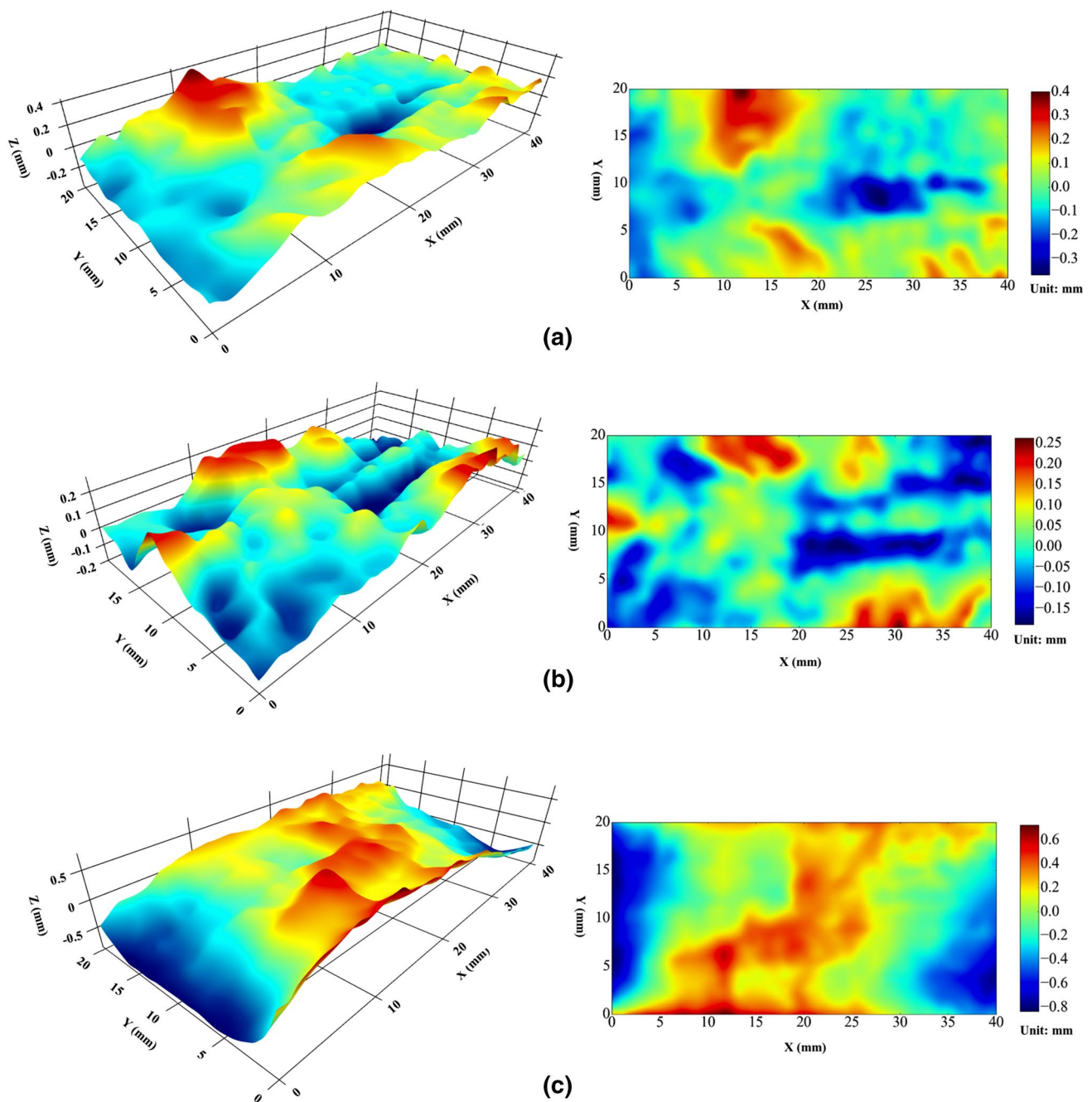
Fig. 7 Heat map of the fractured surfaces: **a** sample no. 1; **b** sample no. 2; and **c** sample no. 3

nonlinear as shown in Fig. 9, which present the results of the sample no. 2. Such a phenomenon can lead to an overestimation of the gas permeability for high gas pressures. Change of gas flow channels along the fracture surface under high gas pressure would be another factor that greatly influence fracture permeability. The high permeability induced by high gas pressures should be further investigated in the future.

Conclusions

To investigate the stress-dependent permeability of natural fractured shale, a series of gas permeability tests were carried out under loading and unloading conditions. The results show that the permeability of the fractured shale decreases with increasing hydrostatic stress re-increases
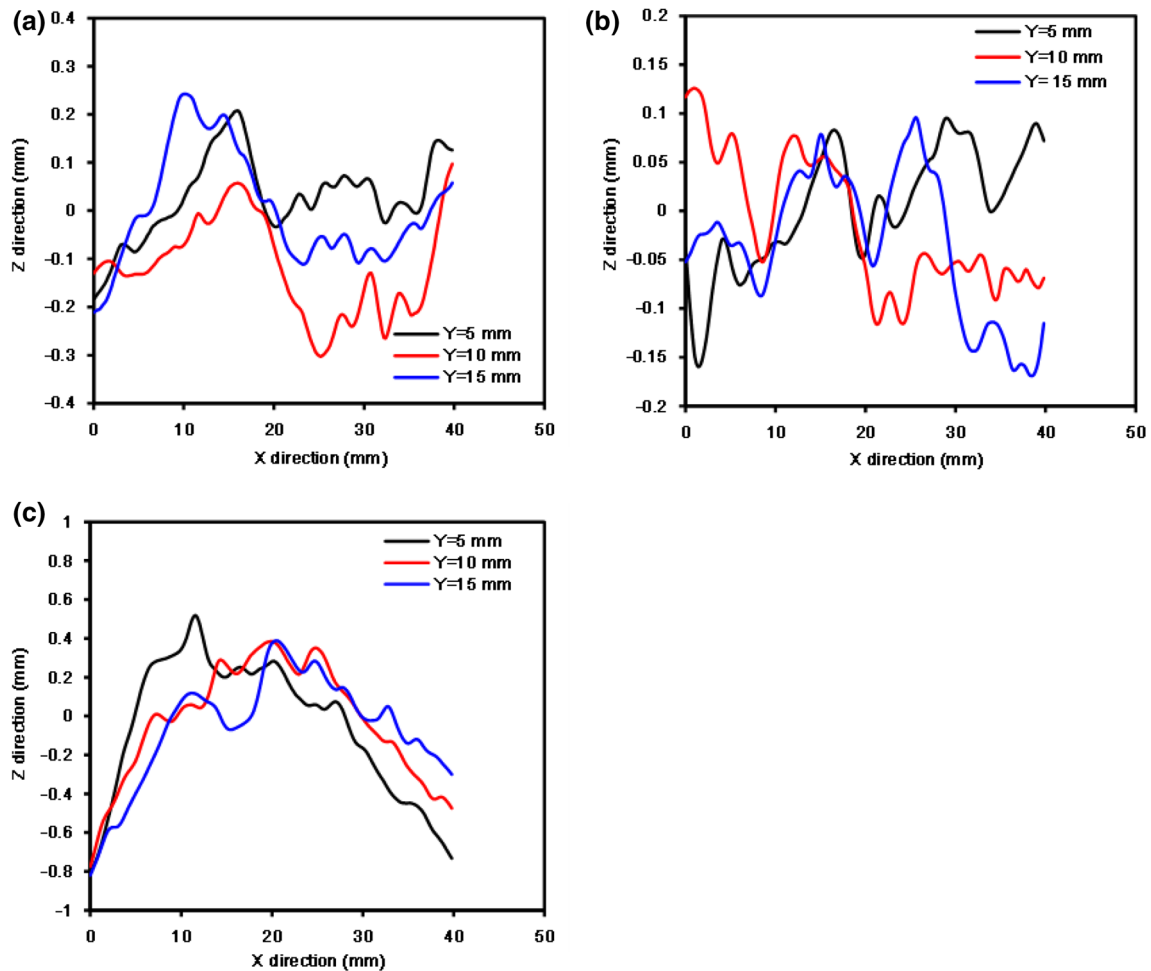
Fig. 8 Selected profiles of the fractured surfaces: **a** sample no. 1; **b** sample no. 2; and **c** sample no. 3
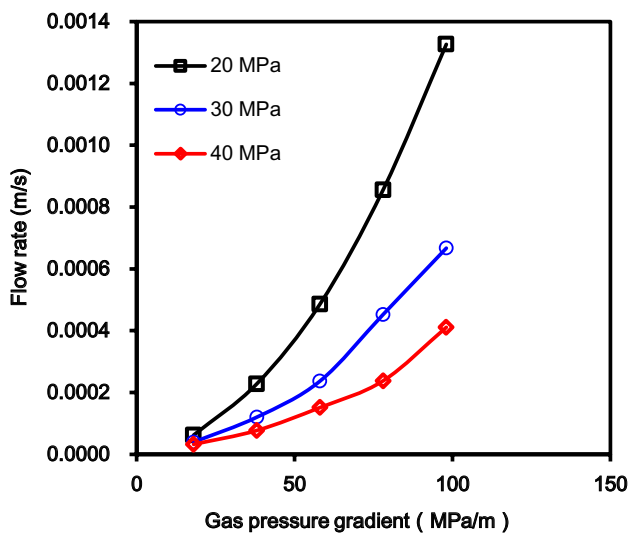

Fig. 9 Flow rate versus gas pressure gradient curves of sample no. 2 under a constant hydrostatic stress

during unloading and is irreversible during loading and unloading. The gas pressure exhibits a significantly larger effect on permeability compared with the hydrostatic stress. A small gas pressure change (e.g., 2 MPa) induces a comparable change in the permeability with a large hydrostatic stress change (e.g., 40 MPa). The nonlinear relationship between the flow rate and gas pressure gradient leads to an overestimation of the gas permeability. The aperture of fractures was estimated by recording the volume change during loading and shows that the aperture change is consistent with the permeability evolution during loading. The fractured surfaces were scanned, and the smoother surfaces exhibited a lower permeability.

Compliance with ethical standards

Conflict of interest The authors declare that they have no competing financial interest.

References

Barton N, Bandis S, Bakhtar K (1985) Strength, deformation and conductivity coupling of rock joints. Int J Rock Mech Min Sci 22(3):121–140

Carey JW, Zhou L, Esteban R, Hiroko M, Hari V (2015) Fracture-permeability behavior of shale. J Unconv Oil Gas Resour 11:27–43

Chen D, Zhenjun P, Ye Z (2015) Dependence of gas shale fracture permeability on effective stress and reservoir pressure: model match and insights. Fuel 139:383–392

Cho Y, Apaydin O, Ozkan E (2013) Pressure-dependent natural-fracture permeability in shale and its effect on shale-gas well production. SPE Reservoir Eval Eng 16:216–228

Davy CA, Skoczylas F, Barnichon J-D, Lebon P (2007) Permeability of macro-cracked argillite under confinement: gas and water testing. Phys Chem Earth Parts A/B/C 32(8–14):667–680. https://doi.org/10.1016/j.pce.2006.02.055

Dong JJ et al (2010) Stress-dependence of the permeability and porosity of sandstone and shale from TCDP Hole-A. Int J Rock Mech Min Sci 47(7):1141–1157

Figueiredo B, Tsang CF, Rutqvist J, Niemi A (2015) A study of changes in deep fractured rock permeability due to coupled hydromechanical effects. Int J Rock Mech Min Sci 79:70–85

Gale JFW, Reed RM, Holder J (2007) Natural fractures in the Barnett shale and their importance for hydraulic fracture treatments. AAPG Bull 91(4):603–622

Gutierrez M, Øino LE, Nygård R (2000) Stress-dependent permeability of a demineralised fracture in shale. Mar Pet Geol 17(8):895–907

Gutierrez M, Katsuki D, Tutuncu A (2015) Determination of the continuous stress-dependent permeability, compressibility and poroelasticity of shale. Mar Pet Geol 68:614–628

Hakami E, Larsson E (1996) Aperture measurements and flow experiments on a single natural fracture. Int J Rock Mech Min Sci Geomech Abstr 33(4):395–404

Hofmann H, Blocher G, Milsch H, Babadagli T, Zimmermann G (2016) Transmissivity of aligned and displaced tensile fractures in granitic rocks during cyclic loading. Int J Rock Mech Min Sci 87:69–84

Li YR, Huang RQ (2015) Relationship between joint roughness coefficient and fractal dimension of rock fracture surfaces. Int J Rock Mech Min Sci 75:15–22

Lu Z, Fang R, Yao H, Dong C, Xian S (2018a) Dynamic responses of unsaturated half-space soil to a moving harmonic rectangular load. Int J Numer Anal Meth Geomech 42:1057–1077

Lu Z, Wu X, Hu Z, Xian S, Fang R (2018b) Electric resistance tests on compacted clay material under dynamic load coupled with dry-wet cycling, Adv Mater Sci Eng 5:387–540

Palmer I, Mansoori J (1998) How permeability depends on stress and pore pressure in coalbeds: a new model. SPE Reservoir Eval Eng 1(6):539–544

Ren Y, Qian B, Zhang J et al (2015) Practice and understanding of industrial fracturing for shale gas of Longmaxi Formation in Changning region (in Chinese). Oil Drill Product Technol 37(4):96–99

Sahimi M (1995) Flow and transport in porous media and fractured rock. VCH, Vancouver

Seidle JP, Jeansonne MW, Erickson DJ (1992) Application of matchstick geometry to stress dependent permeability in coals. In: SPE rocky mountain regional meeting, Society of petroleum engineers, Casper, Wyoming, 18–21 May 1992

Smart BGD, Somerville JM, Edlman K, Jones C (2001) Stress sensitivity of fractured reservoirs. J Petrol Sci Eng 29:29–37

Su K, Sanz Perl Y, Onaisi A, Pourpark H, Vidal-Gilbert S (2017) Experimental study of hydromechanical behavior of fracture of Vaca Muerta Gas Shale, ARMA 2017-857, June 2017

Vogler D, Amann F, Bayer P, Elsworth D (2016) Permeability evolution in natural fractures subject to cyclic loading and Gouge formation. Rock Mech Rock Eng 49(9):1–17

Wang S, Elsworth D, Liu J (2011) Permeability evolution in fractured coal: the roles of fracture geometry and water-content. Int J Coal Geol 87(1):13–25

Wu W, Reece JS, Gensterblum Y, Zoback MD (2017) Permeability evolution of slowly slipping faults in shale reservoirs. Geophys Res Lett, 44(22):56

Xiong X, Li B, Jiang Y, Koyama T, Zhang C (2011) Experimental and numerical study of the geometrical and hydraulic characteristics of a single rock fracture during shear. Int J Rock Mech Min Sci 48(8):1292–1302

Yang D et al (2017) Experimental investigation on the coupled effect of effective stress and gas slippage on the permeability of shale. Sci Rep 7:44696. https://doi.org/10.1038/srep44696

Ye Z, Janis M, Ghassemi A, Riley S (2017) Laboratory investigation of fluid flow and permeability evolution through shale fractures. In: Unconventional Resources Technology Conference, Austin, Texas. Society of Exploration Geophysicists, American Association of Petroleum Geologists, Society of Petroleum Engineers, 24–26 July 2017 (pp. 2038–2052)

Zhang CL (2013) Sealing of fractures in claystone. J Rock Mech Geotech Eng 5:214–220

Zhou T, Zhang SC, Feng Y, Shuai YY, Zou YS, Li N (2016) Experimental study of permeability characteristics for the cemented natural fractures of the shale gas formation. J Nat Gas Sci Eng 29:345–354